Chemical Science

ROYAL SOCIETY OF CHEMISTRY

EDGE ARTICLE

View Article Online
View Journal

Cite this: DOI: 10.1039/d6sc02898e

All publication charges for this article have been paid for by the Royal Society of Chemistry

Unraveling emission narrowing pathways in N-embedded polyaromatic systems *via* sequential π-interlocking for efficient electroluminescence

Danish Khan,[a] Seungwon Han,[b] Keerthika P,[d] Pankaj Kumar Gupta,[a] Ankit Kumar,[a] Jun Yeob Lee *[bc] and Rajendra Kumar Konidena *[a]

The growing demand for complex B-free, narrowband organic emitters has garnered significant attention for OLEDs, but preparing them remains challenging due to limited control over vibronic coupling and structural relaxation. Herein, we present a streamlined molecular design strategy based on sequential π-interlocking to regulate the emission bandwidth in N-embedded polyaromatic hydrocarbons (N-PAHs). A library of emitters (**CzTPA**, **CzCz**, **CzICz**, and **ICzICz**), each containing two N-atoms and six phenyl rings, was constructed with progressively increasing degrees of π-interlocking from mono-to four-fold fused architectures. Combined photophysical and density functional theory studies reveal that stepwise π-interlocking significantly rigidifies molecular geometry, suppresses vibronic coupling, and minimizes structural relaxation. Consequently, the emission bandwidth gradually narrows across the series, leading to a significant shift from 58 to 24 nm in FWHM from mono-fused **CzTPA** to four-fold fused **ICzICz**, accompanied by a blue-shifted emission. Notably, each π-interlocking contributes to an ∼9–14 nm narrowing of the FWHM. The **ICzICz** exhibits the lowest reorganization energy, a narrow FWHM of ∼24 nm, and a high PLQY of ∼92%. OLEDs based on **ICzICz** deliver pure ultra-violet emission with an EQE of 4.2% and CIEy of ∼0.029. As a host for the green phosphor, the device achieves an EQE of ∼18.5% with an extremely low roll-off (∼1%) at 3000 cd m^{-2}. This work establishes a general molecular design tool-kit for producing efficient B-free narrowband organic emitters for OLEDs.

Received 8th April 2026
Accepted 1st June 2026

DOI: 10.1039/d6sc02898e

rsc.li/chemical-science

Introduction

Driven by the promise of next-generation ultra-high-definition (UHD) displays, organic light emitting diodes (OLEDs) with high efficiency and superior color purity have attracted tremendous attention.[1–3] To meet these cutting-edge requirements, it is highly essential to develop organic emitters with extremely narrow full-width-at-half-maximum (FWHM < 30 nm) emission.[1–6] Indeed, they can effectively eliminate the need for additional color filters in OLEDs to obtain pure colors, thereby reducing device complexity, minimizing power consumption, and preventing emission energy loss as well as efficiency deterioration.[1–6] Although conventional organic luminophores offer notable advantages over metal-based phosphorescent emitters, their strong vibronic coupling and significant structural relaxation during electronic transitions from the ground (S_0) to the excited state (S_1) typically result in broad FWHM > 60 nm.[7–9] Suppressing vibrational relaxation by rigidifying the molecular framework is a classical strategy to narrow the FWHM.[10–14] However, conventional fused polyaromatic hydrocarbons (PAHs) such as perylene, anthracene, *etc.* typically display broad emission characterized by multiple vibronic peaks.[15,16] As a result, these systems generally exhibit large FWHM and low electroluminescence (EL) efficiencies. Therefore, the development of streamlined molecular design strategies capable of delivering organic emitters with narrow FWHM < 30 nm and high efficiency remains highly desirable for the advancement of next-generation high-color-purity OLEDs.

To this end, molecular design strategies that incorporate non-bonding orbital characteristics and enable spatial separation of the highest occupied molecular orbital (HOMO) and the lowest unoccupied molecular orbital (LUMO) at the atomic level have been developed.[10–14] One successful approach involves embedding heteroatoms with opposite resonance effects into PAHs to generate narrowband emission. In this context, multiple-resonance (MR) emitters, particularly those containing *ortho*-positioned boron (B) and nitrogen (N) atoms, have shown remarkable progress.[17–19] In typical B,N-based MR systems, the complementary resonance effects introduced by mutually *ortho*-

[a]*Organic Materials Laboratory (OM-Lab), Department of Chemistry, Indian Institute of Technology-Patna, Bihta Kanpa Rd, Patna, Dayalpur Daulatpur, Bihar 801106, India. E-mail: rajsan@iitp.ac.in; rkonidena531@gmail.com*

[b]*School of Chemical Engineering, Sungkyunkwan University 2066, Seobu-ro, Jangan-gu, Suwon, Gyeonggi, 16419, Korea. E-mail: leej17@skku.edu*

[c]*SKKU Institute of Energy Science and Technology, Sungkyunkwan University, 2066, Seobu-ro, Jangan-gu, Suwon, Gyeonggi, 16419, Republic of Korea*

[d]*Department of Chemistry, Faculty of Engineering and Technology, SRM Institute of Science and Technology, Kattankulathur, , Chengalpattu, Tamil Nadu 602 203, India*

or *para*-positioned B and N atoms induce localized frontier molecular orbitals within the PAH backbone.[10–14] This atomic-level separation of the HOMO and LUMO results in short-range charge-transfer (SRCT) excited states, effectively suppressing vibronic coupling. Consequently, such emitters can deliver narrowband emission with FWHM < 30 nm along with high photoluminescence quantum yields (PLQYs). Despite these promising characteristics, B,N-doped PAHs demand complicated synthesis, typically involving alkyl lithium mediated B-incorporation, which can lead to limited yields and synthetic challenges.[3,20,21] Furthermore, achieving ultraviolet (UV) emission with CIEy < 0.03 remains difficult due to their intrinsic SRCT.[22,23] As an alternative strategy, Lee *et al.* demonstrated an interesting core, indolo[3,2,1-*jk*]carbazole (ICz), a N-centered tripod structure surrounded by three aromatic rings, in which the MR effect can also be generated through the difference in electronegativity between C and N atoms.[24] This design enables effective separation of the HOMO and LUMO across different carbon atoms without the need for B-atoms.[25,26] Importantly, these B-free ICz-based PAHs are synthetically more accessible and have demonstrated exceptionally narrow emission with FWHM as small as ∼10 nm.[25–37] Following this, a considerable number of studies have explored this emerging class of B-free narrowband emissive N-PAHs. Structural modifications have been achieved by introducing various donor or acceptor substituents on the ICz core or by extending the π-backbone through fusion of multiple ICz units, thereby expanding structural diversity and improving OLED performance.[27–37] For example, Zhang and Duan *et al.* reported ICz-based PAHs by arranging N-atoms para to each other (pICz), further modified by incorporating additional triphenylamine units, which resulted in deep-blue emission with a narrow FWHM of 18 nm.[38] Subsequently, the same group developed naphthalene-fused ICz scaffolds to engineer orbital symmetry and extend π-conjugation, enabling ultra-narrowband green emission with an FWHM of 13 nm.[39] More recently, our group reported an ICz system integrated with a carbazole unit at the C4-position, achieving UV emission with an FWHM of 17 nm.[23] Nevertheless, in many ICz-based reported systems, the emission FWHM tends to broaden, indicating that a clear molecular design principle for maintaining narrow emission is still lacking. Therefore, a systematic investigation focusing on how structural rigidification, particularly through the sequential π-interlocking of aromatic units, affects the emission bandwidth is essential for deepening the understanding of molecular design principles governing B-free narrowband N-PAH emitters. Thus, the development of an intelligent molecular design strategy involving a library of structurally related emitters would be highly valuable for establishing clear structure–property relationships and a "*design tool-kit*" for next-generation narrowband organic emitters.

In this work, we aim to elucidate how sequential fusion of aromatic units in π-conjugated scaffolds influences the electronic transitions and emission bandwidth. A systematic molecular library consisting of **CzTPA**, **CzCz**, **CzICz**, and **ICzICz** was developed, where each emitter contains two N-atoms and six phenyl rings, but differs in the degree of phenyl interlocking within the π-framework. Comprehensive structure–property relationships were established through detailed photophysical measurements supported by density functional theory (DFT) calculations. Photophysical studies reveal that the gradual interlocking of phenyl rings, from a mono-fusion in **CzTPA** to a four-fold fused emitter in **ICzICz**, leads to a pronounced narrowing of the emission profile. Across the series, the FWHM decreases by *ca.* 34 nm, accompanied by a pronounced blue-shift. This trend is primarily attributed to the progressive suppression of vibronic coupling in the excited state and reduction in the number of vibrational modes at the low and high frequency regions as the molecular framework becomes more rigid with increasing fusion. The computational analysis further supports this observation; the **ICzICz** exhibits significantly lower reorganization energies (λ_s ∼0.12 eV) and reduced structural relaxation between the ground and excited states compared to the **CzTPA** (λ_s ∼274.8 eV). Notably, each additional phenyl fusion contributes to a *ca.* 9–14 nm narrowing of the FWHM, along with a concomitant decrease in λ_s. Progressive fusion from mono-to four-interlocked architectures enables effective fine-tuning of PLQY, culminating in **ICzICz** with 92%. The OLED based on **ICzICz** exhibited the best performance, with an EQE of 4.2% and pure UV emission (CIEy ≈ 0.029). As a host for the green phosphor, the **ICzICz**-based device achieved an EQE of 18.5%, along with an extremely low efficiency roll-off of ∼1% at a maximum luminance of 3000 cd m^{-2}.

Results and discussion

The synthesis of the target molecules is outlined in Scheme S1. The key intermediate 9-(4-bromophenyl)-3,6-di-*tert*-butyl-9*H*-carbazole (**1**) was subjected to palladium-catalyzed Suzuki coupling with the corresponding boronic acids of triphenylamine (TPA), carbazole (Cz), and ICz to afford **CzTPA**, **CzCz**, and **CzICz**, respectively. Similarly, 11-bromo-2,5-di-*tert*-butylindolo[3,2,1-*jk*]carbazole (**2**) was reacted with the ICz boronic acid under the above-mentioned conditions to yield **ICzICz**. All compounds were thoroughly characterized by NMR spectroscopy and HRMS methods. To obtain materials with high purity suitable for OLED fabrication, vacuum train sublimation was employed. Thermogravimetric analysis (TGA) revealed excellent thermal stability for all compounds, exhibiting decomposition temperatures corresponding to 10% weight loss (T_{10d}) above 400 °C (Fig. S1). Such remarkable thermal robustness is attributed to the rigid molecular building blocks, which enhance structural stability and make them well suited for OLED fabrication.

The molecular design of this work aims to establish a clear understanding of how aromatic π-fusion in organic emitters influences vibronic coupling and excited-state structural reorganization, ultimately narrowing the emission FWHM. The design strategy and computational results are illustrated in Fig. 1. The molecules contain two N-atoms and six phenyl units. Sequential interlocking of the aromatic units from **CzTPA** to **ICzICz**, corresponding to mono-to four-fold fused architectures, was anticipated to progressively suppress structural relaxation and vibronic coupling during the $S_0 \rightarrow S_1$ excitation process,

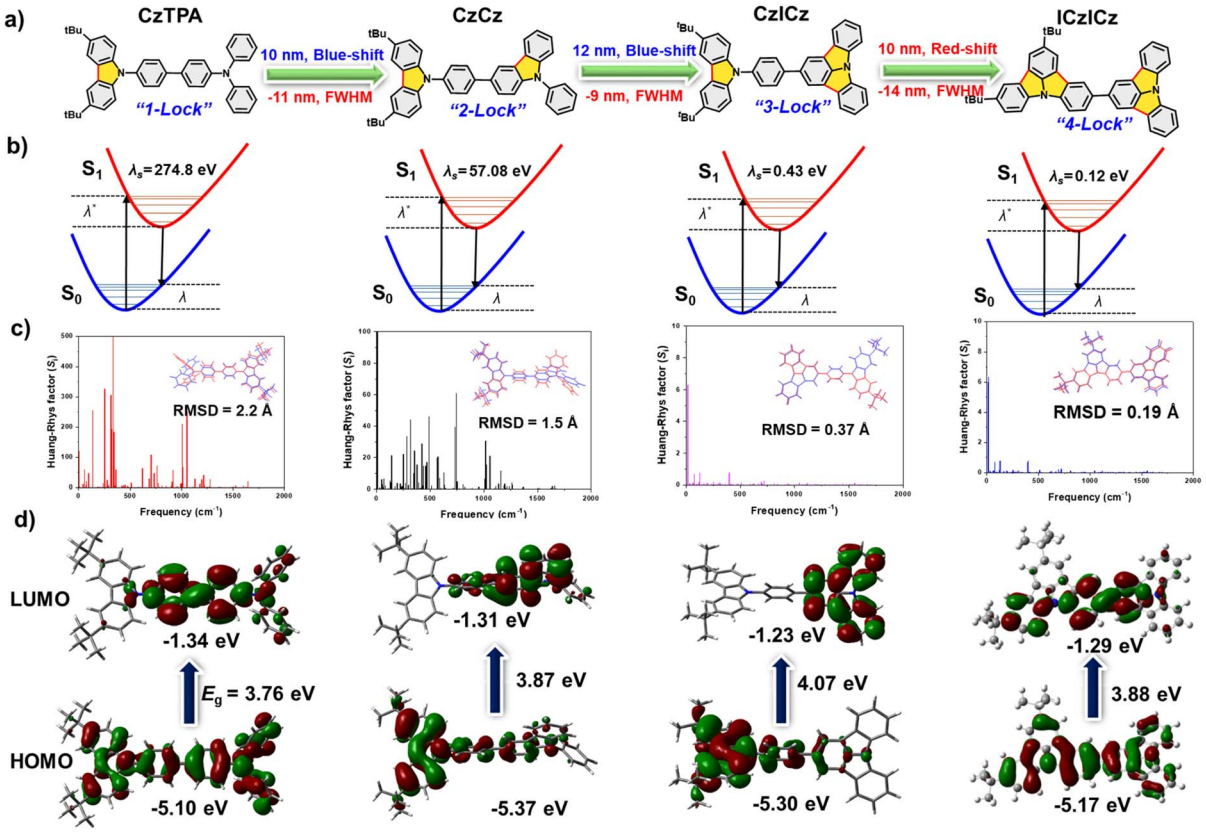

Fig. 1 (a) Molecular design, (b) reorganization energies, (c) Huang–Rhys (HR) frequencies, and (d) frontier molecular orbital (FMO) distribution of the compounds computed by DFT methods.

thereby narrowing the emission bandwidth. This design enables systematic evaluation of the impact of each phenyl fusion in ICz-based N-PAHs on the FWHM, providing insight into the development of this emerging class of emitters. In addition, fusion-induced excited-state electronic redistribution can fine-tune the emission wavelengths. To understand the mechanism responsible for emission narrowing, DFT and time-dependent DFT (TD-DFT) calculations were performed at the B3LYP/6-31G(d,p) level using the Gaussian 16 program package. The optimized ground- and excited-state geometries are shown in Fig. S2. As the degree of phenyl fusion increases from **CzTPA** to **ICzICz**, the molecular framework becomes progressively more rigid and π-conjugated in both the ground and excited states. This rigidification reduces geometrical relaxation following excitation. To quantitatively evaluate the vibronic contributions, Huang–Rhys (HR) factors and λ_s were calculated. To deepen the mechanistic understanding of the Huang–Rhys (HR) factor reduction, we analysed the vibrational mode contributions across the series (**CzTPA** to **ICzICz**) and correlated them with the progressive rigidification induced by π-interlocking. Normal mode analysis reveals two principal classes of vibrational modes. Low-frequency modes (<700 cm^{-1}), primarily associated with phenyl ring torsional/rotational/twisting motions and out-of-plane skeletal distortions, contribute significantly to the total HR factor in the mono-locked system; however, as π-interlocking increases from two-fold to four-fold, these torsional degrees of freedom are progressively suppressed due to restricted rotation of peripheral phenyl rings, leading to a marked reduction in low-frequency vibrational reorganization. High-frequency modes (>700 cm^{-1}), mainly arising from C–C stretching vibrations within the conjugated backbone, are also notably affected: in less rigid systems, bond length alternation upon excitation leads to stronger electron-vibration coupling, whereas increased π-interlocking enhances structural rigidity and electronic delocalization, minimizing geometric relaxation between the S_0 and S_1 states and thereby suppressing high-frequency contributions to the HR factor.[25,29,39,40] Consequently, the overall HR factor and total reorganization energies (λ_s) decrease monotonically from **CzTPA** to **ICzICz**, reflecting progressively weaker vibronic coupling between the S_0 and S_1 states due to the locking of flexible phenyl rotations, which possess large dihedral angles between the phenyl units (>40°). This reduction in vibronic coupling directly translates into narrower emission spectra. The calculated root-mean-square deviations (RMSD) between ground- and excited-state geometries and the λ_s follow the trend: **CzTPA** (2.23 Å/274.87 eV) > **CzCz** (1.50 Å/57.08 eV) > **CzICz** (0.37 Å/0.43 eV) > **ICzICz** (0.19 Å/0.12 eV). The drastic decrease in both RMSD and λ_s values clearly demonstrates that π-fusion effectively suppresses excited-state structural relaxation, which correlates directly with the progressive narrowing of the emission FWHM. Frontier molecular orbital analysis shows

Table 1 Summary of photophysical, thermal and electrochemical properties of the compounds

Compounds	λ_{abs},[a] nm	λ_{em},[a] (FWHM) nm	Stokes shift[a] (nm)	Φ_F,%/τ_p, ns[a]	E_T,[b] eV	HOMO,[c] eV	LUMO,[d] eV	E_g,[e] eV	T_{10d},[f] °C
CzTPA	293, 298, 348	410 (58)	62	62/1.02	3.14	−5.44	−2.14	3.30	401
CzCz	298, 348, 375	400 (47)	25	78/6.24	2.91	−5.63	−2.35	3.28	423
CzICz	298, 316, 348	388 (38)	38	86/4.67	2.87	−5.70	−2.41	3.29	411
ICzICz	298, 348, 375	398 (24)	24	91/6.29	2.80	−5.78	−2.48	3.30	402

[a] Measured in dilute DCM solution. τ_p, lifetime of the samples. [b] Lowest excited triplet energies (E_T) estimated from phosphorescence spectra. [c] Estimated from CV. [d] Calculated by subtracting the HOMO from the optical band gap. [e] Optical band gap. [f] Thermal decomposition temperature of 10% weight loss.

that in **CzTPA** and **CzCz**, the HOMO is delocalized across the molecular backbone, while the LUMO is primarily localized on the central phenyl unit with partial contribution from the chromophore. In **CzICz**, the HOMO resides on the carbazole unit and the LUMO is centered on the ICz core. In contrast, **ICzICz** exhibits HOMO and LUMO orbitals delocalized over the entire molecule, indicative of MR-type character. The HOMO energy gradually decreases from −5.10 eV (**CzTPA**) to −5.17 eV (**ICzICz**), reflecting the reduced donor strength of the TPA and carbazole units upon π-fusion in ICz. Consequently, the band gap (E_g) can be tuned to achieve deep-violet emission through enhanced molecular rigidification.

The photophysical properties of the compounds were investigated in dilute dichloromethane solutions (1×10^{-5} M). A summary of photophysical properties is provided in Table 1. The absorption spectra display multiple bands in the 290–390 nm region (Fig. 2). The high-energy absorption bands (<350 nm) originate from localized π–π* transitions of the chromophoric units, whereas the lower-energy bands (>370 nm) correspond to delocalized *n*–π*/π–π* transitions across the molecular framework. Among the series, **ICzICz** exhibits the most red-shifted absorption, which can be attributed to the extended π-conjugation between the two π-fused ICz units. The emission of the compounds spans the UV to blue region. **CzTPA** shows the most red-shifted emission in the series (λ_{em} = 410 nm) with a relatively broad FWHM of 58 nm, which can be attributed to the presence of flexible phenyl units that promote excited-state structural relaxation. Upon interlocking one phenyl unit in the TPA core, **CzCz** exhibits a concomitant blue-shift of ∼10 nm along with a narrowed emission band (FWHM = 47 nm). Further π-fusion in **CzICz** results in a more pronounced blue-shift of 22 nm relative to **CzTPA** and additional narrowing of FWHM = 38 nm. In the fully fused **ICzICz** system, four-fold interlocking leads to the narrowest emission in the series with a FWHM of 24 nm. Notably, the emission of **ICzICz** is slightly red-shifted compared to **CzICz**, which can be attributed to the extended π-conjugation between the two ICz fragments (Fig. 2). Overall, the sequential interlocking of flexible phenyl units from **CzTPA** to **ICzICz** leads to a significant reduction in FWHM by ∼34 nm (Fig. 3), reflecting the progressive rigidification of the molecules and the suppression

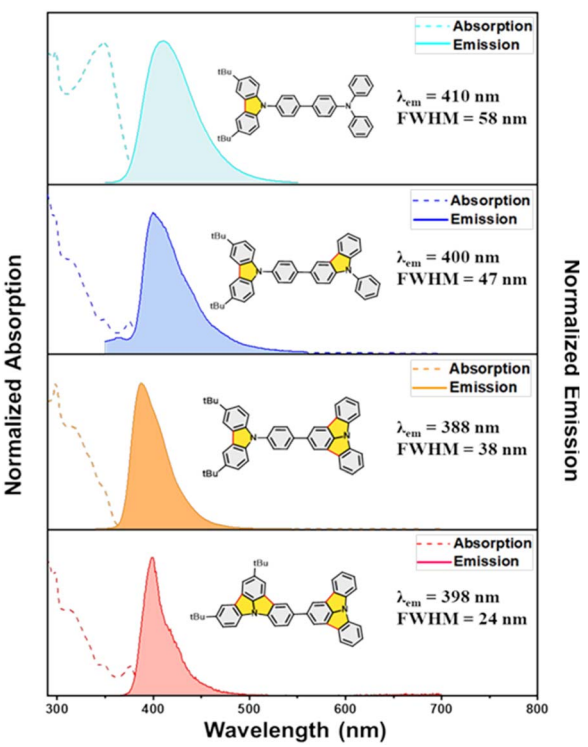

Fig. 2 Absorption and emission spectra of the compounds recorded in dilute dichloromethane.

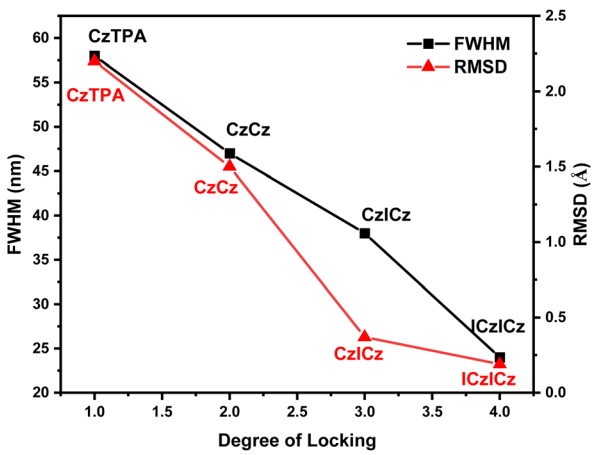

Fig. 3 Degree of π-interlocking *vs.* RMSD (Å) and FWHM (nm) of the emitters.

Table 2 EL data for **CzCz**, **CzICz** and **ICzICz** compounds as emitters and hosts

Compound		Dopant conc. [%]	CE_{max} [cd A^{-1}]	PE_{max} [lm W^{-1}]	EQE_{max} [%]	λ_{EL} [nm]	CIE (x, y)
CzCz	Emitter	20	0.5	0.4	3.2	394	0.18, 0.06
	Host	5	57.5	32.6	16.6	514	0.28, 0.63
CzICz	Emitter	20	0.4	0.3	3.2	402	0.16, 0.024
	Host	5	59.5	37.4	17.2	514	0.29, 0.63
ICzICz	Emitter	20	1.2	1.3	4.2	406	0.15, 0.029
	Host	5	66.1	51.3	18.5	515	0.28, 0.63

of excited state structural relaxation, which is inconsistent with the computational results (*vide supra*). The reduced structural relaxation is further evidenced by the substantial decrease in the Stokes shift from 62 nm for **CzTPA** to 24 nm for **ICzICz**. Notably, each phenyl interlocking step contributes to a *ca.* 9–14 nm narrowing of the emission bandwidth, highlighting the critical role of π-fusion in regulating vibronic coupling and the emission band. To further probe the nature of the excited states, solvatochromic studies were conducted by varying solvent polarity from non-polar cyclohexane to polar DMF (Fig. S3). **CzTPA** exhibits a pronounced bathochromic shift (λ_{em}(CH-DMF) ∼39 nm) with increasing solvent polarity, accompanied by a transformation from structured emission to a broad, structureless profile. This behavior indicates a polar excited state arising from significant structural reorganization and electronic redistribution. In contrast, increasing the degree of phenyl interlocking progressively suppresses this solvent dependence. The fully fused **ICzICz** displays negligible solvatochromic shift, suggesting the presence of a rigidified framework. The Lippert–Mataga plot shows an almost linear slope for the **CzICz** and **ICzICz**, which indicates less pronounced electronic redistribution (Fig. S4). The fluorescence lifetime studies reveal single exponential decay with time scale in the range of 1.02–6.29 ns. Within the series, all molecules except **CzTPA** show comparable lifetimes in the range of 4.67–6.29 ns, suggesting similar singlet exciton dynamics and radiative decay behavior. The observed short lifetime for **CzTPA** (1.02 ns) can be attributed to the enhanced CT character of the excited state, which is also evident from its relatively strong solvatochromic shift (Fig. S3). The absolute PLQY, measured using an integrating sphere, increased progressively from **CzTPA** (62%) to **ICzICz** (92%), indicating reduced non-radiative decay pathways upon increased molecular rigidification. To evaluate their potential as host for PhOLEDs, the triplet energy levels (E_T) were determined from phosphorescence spectra measured in frozen THF at 77 K (Fig. S5). All compounds exhibit high triplet energies (>2.80 eV), which are significantly higher than that of green phosphor, $Ir(ppy)_3$, ∼2.49 eV. These high triplet energies ensure efficient energy transfer to the emitter while suppressing detrimental back-energy transfer.

The electrochemical properties were investigated by cyclic voltammetry (CV) in dilute dichloromethane solution using tetrabutylammonium perchlorate as the supporting electrolyte, with ferrocene employed as the internal reference (Fig. S7). The compounds exhibit an oxidation wave at a potential positively shifted relative to the ferrocene, attributed to the removal of electrons from the chromophores. A systematic increase in oxidation potential is observed across the series as the degree of aromatic π-interlocking increases from **CzTPA** to **ICzICz**. This trend arises from the gradual decrease in donor strength of the chromophoric units. **CzTPA** displays the lowest oxidation onset potential (1.04 V), consistent with the strong electron-donating nature of the TPA unit. In **CzCz** and **CzICz**, the electron-donating centre shifts to the carbazole moiety following phenyl fusion, which possesses weaker donor ability compared with TPA. Consequently, these compounds exhibit higher oxidation potential than **CzTPA**. In contrast, the fully fused **ICzICz** system shows the highest oxidation potential (1.38 V) in

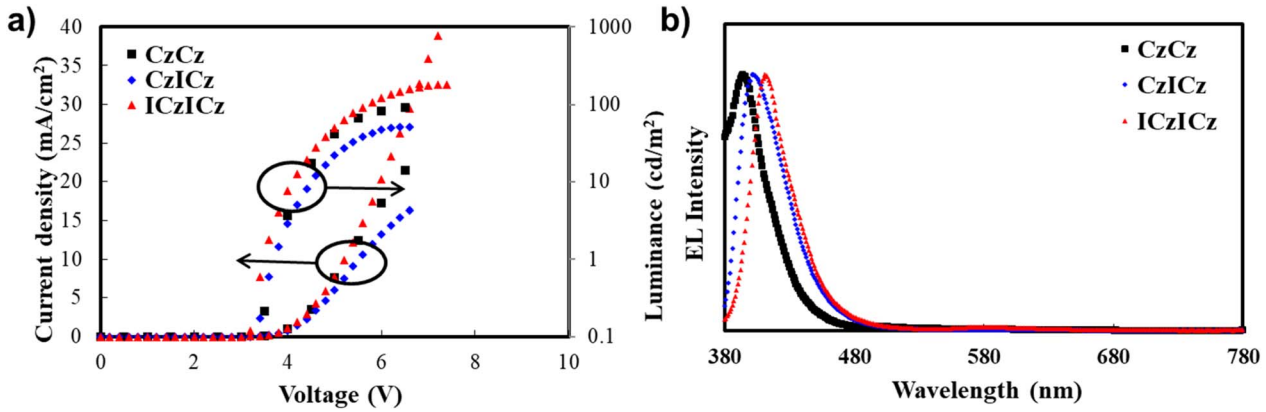

Fig. 4 (a) I–V–L and (b) EL plots of the 20 wt% doped OLED device.

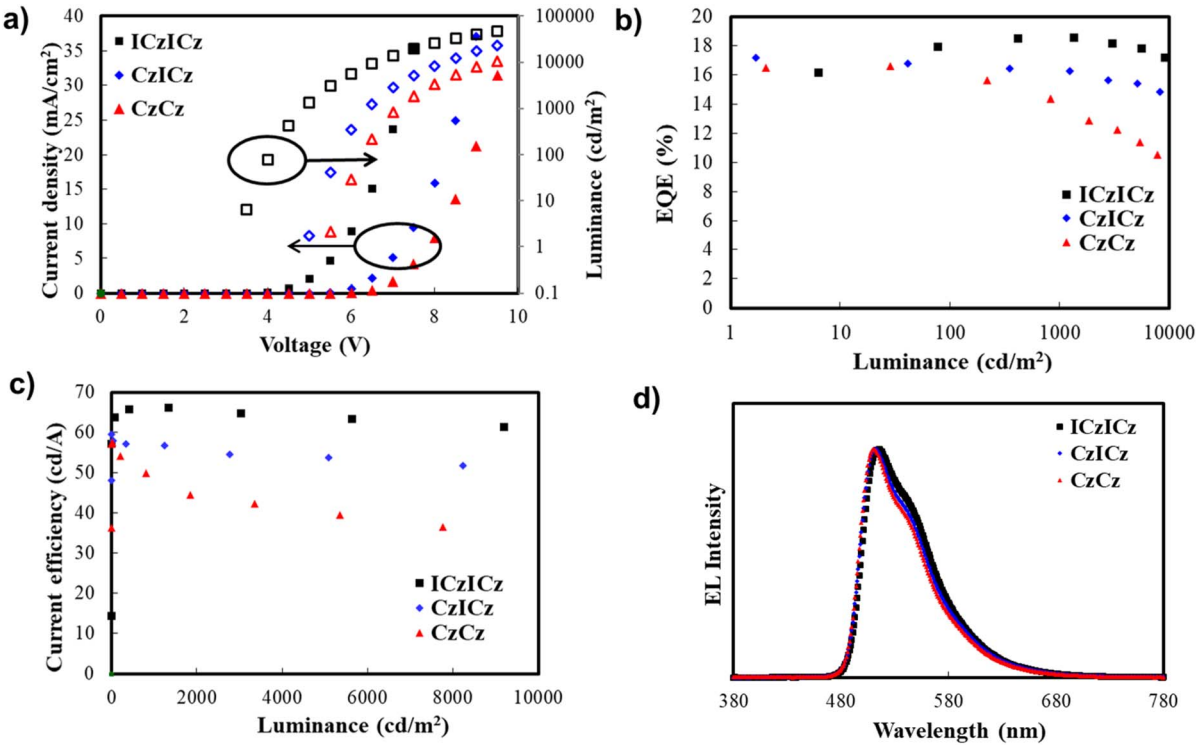

Fig. 5 (a) I–V–L; (b) EQE *vs.* L; (c) CE *vs.* L and (d) EL plots of the PhOLEDs.

the series, reflecting the relatively weak electron-donating character of the ICz unit. Accordingly, the HOMO energy level follow the trend: **CzTPA** (−5.44 eV) < **CzCz** (−5.63 eV) < **CzICz** (−5.70 eV) < **ICzICz** (−5.78 eV). The LUMO energies were estimated by subtracting the HOMO energies from the optical band gap and fall within the range of 2.14–2.48 eV.

The applicability of these materials initially was tested as dopant emitters in OLEDs in the configuration: PEDOT:PSS (40 nm)/TAPC (10 nm)/TCTA (5 nm)/mCP (5 nm)/EML (30 nm)/TSPO1 (25 nm)/LiF (1.5 nm)/Al (200 nm), where the emitting layer (EML) consisted of 20 wt% emitter doped in a DPEPO host. The OLED device structure is shown in Fig. S8 and S9. A summary of EL properties is provided in Table 2. The EL spectra of the devices fall in the near-UV region and closely match the corresponding PL spectra measured in solution, confirming that the emission originates from the desired emitting layer. Among the series, **CzICz** and **ICzICz** exhibit pure UV emission with CIEy ∼0.024 and 0.029, respectively, which can be attributed to their narrowband emission. The significance of π-interlocking in improving the color purity is evident by comparing **ICzICz** with the reported emitters (Table S1). Overall, the **ICzICz**-device demonstrates the best performance in the series, delivering a maximum EQE of 4.2% in the deep-UV region (Fig. 4). This enhanced performance can be attributed to its high PLQY and improved charge mobility. Furthermore, the wide energy gap, high triplet energy, E_T > 2.80 eV and thermal stability motivated us to use these materials as host materials for green phosphor, $Ir(ppy)_3$. The PhOLED devices were fabricated with the structure: PEDOT:PSS/TAPC (20 nm)/PCzAc (10 nm)/host:$Ir(ppy)_3$ (25 nm, 5 wt%)/TSPO1 (5 nm)/TPBi (40 nm)/LiF (1.5 nm)/Al (200 nm). The diodes fabricated based on **CzCz**, **CzICz**, and **ICzICz** showed EQE/CE/PE values of 16.6%/57.5 cd A^{-1}/32.6 lm W^{-1}, 17.2%/59.5 cd A^{-1}/37.4 lm W^{-1}, and 18.5%/66.1 cd A^{-1}/51.3 lm W^{-1}, respectively (Fig. 5). Notably, the **ICzICz**-based device also exhibits excellent efficiency stability, maintaining an EQE of 18.3% at a luminance of 3000 cd m^{-2} with only 1.0% efficiency roll-off. It is evident that as π-interlocking increases from **CzCz** to **ICzICz**, the device EQE improves while efficiency roll-off is effectively suppressed. This trend can be directly correlated with the increasing degree of interlocking, which reduces the E_T gap between the host and dopant, thereby enabling more efficient energy transfer. Simultaneously, increased π-interlocking enhances molecular planarization and reduces the LUMO energy, which could facilitate efficient charge transport within the device (Fig. S10).[41,42] This is further supported by the comparison of the current density and luminance characteristics shown in Fig. 5. As the degree of interlocking increases from **CzCz** to **ICzICz**, both the current density and luminance increase significantly at lower V_{on}, indicating better charge mobility, efficient charge recombination and exciton formation within the device. Consequently, the four-fold interlocked **ICzICz** could exhibit more efficient energy transfer from host to guest along with balanced charge transport within the device, leading to superior device performance. These results highlight the effectiveness of the multiple interlocking strategy in developing rigid, high-triplet energy materials as promising dual functional materials for high-performance OLEDs.

Conclusion

In conclusion, we demonstrate a streamlined molecular design strategy based on step-wise aromatic π-interlocking to establish an emission narrowing mechanism by regulating vibronic coupling and excited-state structural relaxation in B-free organic emitters. The sequential interlocking from **CzTPA** to **ICzICz** results in a significant blue-shift of the emission toward the UV region, accompanied by a substantial narrowing of the emission FWHM by ∼34 nm. Notably, each phenyl fusion contributes to a *ca.* 10–14 nm reduction in the FWHM, ultimately yielding **ICzICz** as the narrowest emitter in the series with a FWHM of 24 nm and a pure UV-emission, with λ_{em} ∼398 nm. DFT studies reveal a dramatic decrease in the λ_s/RMSD of 274 eV/2.2 Å for **CzTPA** to 0.14 eV/0.19 Å for **ICzICz**, confirming that sequential π-fusion effectively suppresses vibronic coupling and structural distortion in the excited state, which is further corroborated by solvatochromic studies. The four-fold fused **ICzICz** demonstrates the best OLED performance, achieving an EQE of 4.2% with pure UV emission (CIEy ≈ 0.029). As a host for green phosphor, the device achieves an EQE of 18.5% with an extremely low efficiency roll-off of only 1% at 3000 cd m^{-2}. These results highlight the critical role of the systematic π-fusion strategy for the development of high-performance organic emitters for OLEDs.

Author contributions

Danish Khan: synthesis, characterization and data curation; Pankaj Kumar Gupta: synthesis; P. Keerthika and Ankit Kumar: photophysics; Seungwon Han: OLED device fabrication, testing; Jun Yeob Lee: supervision and editing; Rajendra Kumar Konidena: conceptualization, supervision, manusript writting, funding acquisition, project administration.

Conflicts of interest

There are no conflicts to declare.

Data availability

The data supporting this article have been included as part of the supplementary information (SI). Supplementary information: experimental methods, NMR, photophysical, TGA, CV and OLED data. See DOI: https://doi.org/10.1039/d6sc02898e.

Acknowledgements

DK and AK thanks IIT Patna for fellowship. PK thanks ANRF-NPDF fellowship (PDF/2025/006242). RK acknowledges a PM-ECRG grant (ANRF/ECRG/2025/002769/CS) sponsored by ANRF-India and SAIF facility IIT Patna. JY thanks MOTIE (RS-2024-00418086) and National Research Foundation of Korea (RS-2024-00442755).

References

1 C.-Y. Chan, M. Tanaka, Y.-T. Lee, Y.-W. Wong, H. Nakanotani, T. Hatakeyama and C. Adachi, *Nat. Photonics*, 2021, **15**, 203–207.
2 X. Liu, L. Hua, X. Lai, J. H. Kim, Q. Zhu, J. Y. Lee, W. Zhu and Y. Wang, *Adv. Mater.*, 2025, **37**, 2500690.
3 S. Madayanad Suresh, D. Hall, D. Beljonne, Y. Olivier and E. Zysman-Colman, *Adv. Funct. Mater.*, 2020, **30**, 1908677.
4 M. Mamada, M. Hayakawa, J. Ochi and T. Hatakeyama, *Chem. Soc. Rev.*, 2024, **53**, 1624–1692.
5 L. Xing, R. Sun, W. Chen, Z. Deng, J. Tan, J. Jin, S. Li, S. Ji, Z. Zhao and Y. Huo, *Angew. Chem., Int. Ed.*, 2026, e8746575.
6 D. Zhang, C. Qu, Q. Wang, J. Zhou, M. Mai, Y. Zhang, H. Dai, D. Zhang and L. Duan, *Angew. Chem., Int. Ed.*, 2026, **65**, e25925.
7 W. Qiu, D. Liu, M. Li, X. Cai, Z. Chen, Y. He, B. Liang, X. Peng, Z. Qiao, J. Chen, W. Li, J. Pu, W. Xie, Z. Wang, D. Li, Y. Gan, Y. Jiao, Q. Gu and S.-J. Su, *Nat. Commun.*, 2023, **14**, 2564.
8 J. Zeng, Y. Wu, Z. Chen, J. Qin, X. Guan, L. Xu, X. Dong, B. Z. Tang and Z. Zhao, *Angew. Chem., Int. Ed.*, 2026, **65**, e3521059.
9 C. Liao, S. Wang, B. Chen, Q. Xie, J. Feng, J. Bai, X. Li and H. Liu, *Angew. Chem., Int. Ed.*, 2025, **64**, e202414905.
10 H. J. Kim and T. Yasuda, *Adv. Opt. Mater.*, 2022, **10**, 2201714.
11 H.-Z. Li, F.-M. Xie, Y.-Q. Li and J.-X. Tang, *J. Mater. Chem. C*, 2023, **11**, 6471–6511.
12 J. M. Ha, S. H. Hur, A. Pathak, J.-E. Jeong and H. Y. Woo, *NPG Asia Mater.*, 2021, **13**, 53.
13 J.-M. Teng, Y.-F. Wang and C.-F. Chen, *J. Mater. Chem. C*, 2020, **8**, 11340–11353.
14 P. Keerthika, S. W. Han, A. Kumar, V. Nutalapati, K. R. Naveen, J. Y. Lee and R. K. Konidena, *Chem. Commun.*, 2025, **61**, 12554–12557.
15 T. Noda, H. Sasabe, T. Owada, R. Sugiyama, A. Arai, K. Kumada, H. Tsuneyama, Y. Saito and J. Kido, *Chempluschem*, 2022, **87**, 202100517.
16 Y. Lv, J. Bi, R. Wang, Z. Yang, X. Yang, S. Zhao, S. Wang, H. Liu, S.-T. Zhang and B. Yang, *Chem. Sci.*, 2025, **16**, 22424–22437.
17 R. Ming, Z. Xue, Y. Xu, Z. Zhang, Z. Chen, J. Miao, Z. Huang and C. Yang, *Angew. Chem., Int. Ed.*, 2025, **64**, e202516696.
18 T. Fan, Q. Liu, X. Cao, C. Li, Y. Zhang, H. Zhang and L. Duan, *J. Am. Chem. Soc.*, 2026, **148**, 10744–10752.
19 H. Hirai, K. Nakajima, S. Nakatsuka, K. Shiren, J. Ni, S. Nomura, T. Ikuta and T. Hatakeyama, *Angew. Chem., Int. Ed.*, 2015, **54**, 13581–13585.
20 X. Wang, L. Duan and D. Zhang, *Chem. Eur J.*, 2023, **29**, e202300701.
21 L. Ge, W. Zhang, Y.-H. Hao, M. Li, Y. Liu, M. Zhou and L.-S. Cui, *J. Am. Chem. Soc.*, 2024, **146**, 32826–32836.
22 Y. Liu, S. Li, J. Zhao, W. Ping, Z. Yang, L. Hua, J. Wang, S. Ying, Z. Ren and S. Yan, *Angew. Chem., Int. Ed.*, 2025, **64**, e202513129.

23 A. Kumar, P. Keerthika, S. W. Han, J. Y. Lee and R. K. Konidena, *ACS Mater. Lett.*, 2026, **8**, 544–550.
24 H. L. Lee, W. J. Chung and J. Y. Lee, *Small*, 2020, **16**, 1907569.
25 D. Zhang, Q. Wang, J. Zhou, W. Yuan, C. Cheng, J. Wei, D. Zhang and L. Duan, *Angew. Chem.*, 2025, **137**, e202517349.
26 V. V. Patil, H. L. Lee, I. Kim, K. H. Lee, W. J. Chung, J. Kim, S. Park, H. Choi, W. Son, S. O. Jeon and J. Y. Lee, *Adv. Sci.*, 2021, **8**, 2101137.
27 J. H. Lee, T. Watanabe, L. Hartmann and T. Yasuda, *Angew. Chem., Int. Ed.*, 2025, **64**, e202505191.
28 Y. Im, S. H. Han and J. Y. Lee, *J. Mater. Chem. C*, 2018, **6**, 5012–5017.
29 Y. Wu, S. Zhai, Y. Deng, X. Wang, Z. Bin and J. You, *Angew. Chem., Int. Ed.*, 2025, **64**, e202518763.
30 X. Zeng, X. Wang, Y. Zhang, G. Meng, J. Wei, Z. Liu, X. Jia, G. Li, L. Duan and D. Zhang, *Angew. Chem., Int. Ed.*, 2022, **61**, e202117181.
31 D. Hall, K. Stavrou, E. Duda, A. Danos, S. Bagnich, S. Warriner, A. M. Z. Slawin, D. Beljonne, A. Köhler, A. Monkman, Y. Olivier and E. Zysman-Colman, *Mater. Horiz.*, 2022, **9**, 1068–1080.
32 H. L. Lee, J. Kang, J. Lim, S. C. Kim, S. O. Jeon and J. Y. Lee, *Nat. Commun.*, 2023, **14**, 4818.
33 Q. Peng, W. Yang, N. Li, S. Gong, X. Gao, C. Ye, Y. Zou and C. Yang, *Chem. Eng. J.*, 2023, **466**, 143423.
34 R. Gao, X. Li, X. Tian, R. Yang, Y. Luo, Z. Jia, J. Huang, H. Xu, Y. Miao, H. Wang, J. Li and Z. Zhao, *Chem. Eng. J.*, 2025, **524**, 169570.
35 H. Li, J. Qin, T. Ma, J. Zeng, Z. Chen, Y. Fu, H. Lu, Z. Zhao and X. J. Feng, *Chem. Sci.*, 2026, **17**, 1694–1702.
36 Z. Wang, X. Hu, Z. Yan, J. Liang, X. Song, Q. Chen, H. Bi and Y. Wang, *Adv. Sci.*, 2025, **12**, 2410479.
37 Q. Wang, H. Zhang, J. Zhou, H. Dai, M. Mai, T. Huang, L. Wang, X. Wang, D. Zhang and L. Duan, *Adv. Mater.*, 2025, **37**, 2503839.
38 J. Wei, C. Zhang, D. Zhang, Y. Zhang, Z. Liu, Z. Li, G. Yu and L. Duan, *Angew. Chem., Int. Ed.*, 2021, **60**, 12269–12273.
39 X. Zeng, L. Wang, H. Dai, T. Huang, M. Du, D. Wang, D. Zhang and L. Duan, *Adv. Mater.*, 2023, **35**, 2211316.
40 T. Fan, Q. Liu, G. Zhang, X. Wang, D. Zhang and L. Duan, *Adv. Mater.*, 2024, **36**, 2408816.
41 R. K. Konidena, K. R. J. Thomas, M. Singh and J. H. Jou, *J. Mater. Chem. C*, 2016, **4**, 4246–4258.
42 J. Y. Liu, J. Y. Bai, Z. Zhang, G. Yuan, Y. H. He, Y. C. Wang, Y. Q. Li and J. X. Tang, *Angew. Chem., Int. Ed.*, 2026, **65**, e21715.